Chapter 1

Motivation

Experiment 760 located at Fermi National Accelerator Laboratory (Fermilab) has studied charm antiquark-quark ($\bar{c}c$) bound states, which are called charmonium. E760 was designed not only to study known $\bar{c}c$ resonances, but was also designed to search for and discover new $\bar{c}c$ states. In particular, the experiment's principal purpose is to discover the charmonium $^1\mathrm{P}_1$ (h_c) state. The mass of the $^1\mathrm{P}_1$ is important to understanding the hyperfine structure of bound states in quantum chromodynamics (QCD).

Described in this thesis is the search for the $^1\mathrm{P}_1$ through decays to lower charmonium states:

$$\bar{p}p \rightarrow {}^1\mathrm{P}_1 \rightarrow \quad J/\psi + X \tag{1.1}$$

$$\bar{p}p \rightarrow {}^1\mathrm{P}_1 \rightarrow \quad \eta_c + \gamma. \tag{1.2}$$

The J/ψ and η_c are identified by electromagnetic decay products. In general, E760 searches for charmonium by

$$\bar{p}p \rightarrow \bar{c}c \rightarrow \quad e^+e^- + X \tag{1.3}$$

$$\bar{p}p \rightarrow \bar{c}c \rightarrow \quad \gamma\gamma + X \tag{1.4}$$

where the $e^+e^-(\gamma\gamma)$ invariant mass reconstructs to a $\bar{c}c$ state J/ψ or ψ' (η_c or χ_2) and X can be η, $\pi\pi$, π^o, a gamma ray, or nothing. The $^1\mathrm{P}_1$ radiative decay is also searched for by the η_c decaying to three neutral mesons, which then all subsequently decay to pairs of gamma rays resulting in a 7 gamma ray final state. A further search has involved:

$$\bar{p}p \to {}^1\mathrm{P}_1 \to \quad \eta + \gamma, \tag{1.5}$$

$$\bar{p}p \to {}^1\mathrm{P}_1 \to \quad \eta' + \gamma, \tag{1.6}$$

where the η and η' decay to three neutral mesons and the final state is 7 gamma rays.

The history of charmonium, theoretical expectations for the $^1\mathrm{P}_1$, and previous experimental spectroscopy results are discussed in this chapter. A description of the experimental apparatus is given in chapter 2. A detailed description of the design and construction of the central calorimeter is presented in chapter 3. The trigger system and procedure for data collection are outlined in chapter 4. The central calorimeter's calibration and monitoring are given in chapter 5. Chapter 6 describes the data filtering, reduction and event selection. Efficiencies and acceptances are contained in chapter 7. The results and conclusions are presented in chapter 8. Some of the descriptions (central calorimeter construction, attempted calibration methods, data acquisition procedure and the pile-up routines) are included to provide essentially the only written detailed documentation of these aspects of the experiment.

$$\begin{pmatrix} e \\ \\ \nu_e \end{pmatrix} \begin{pmatrix} \mu \\ \\ \nu_\mu \end{pmatrix} \begin{matrix} -1 \\ \\ 0 \end{matrix}$$

$$\begin{pmatrix} u \\ \\ d \end{pmatrix} \begin{pmatrix} ? \\ \\ s \end{pmatrix} \begin{matrix} +\frac{2}{3} \\ \\ -\frac{1}{3} \end{matrix}$$

Figure 1.1: The quark and lepton doublets before the discovery of the charm quark and the electrical charges of the members.

1.1 History of the Charm Quark

During the 1960's, a fairly successful model of mesons and baryons was based upon the existence of three quarks (u, d, and s representing respectively up, down and strange flavors). The quarks have fractional charge of $+\frac{2}{3}$ (u) or $-\frac{1}{3}$ (d and s). The quarks can be combined to form complimentary doublets to the then known lepton doublets as shown in figure 1.1. From the aesthetical point of view, a fourth quark of charge $+\frac{2}{3}$ would complete the doublets as pointed out by Bjorken and Glashow [1]; a quark-lepton symmetry would exist and if each quark flavor has three colors (see the next section), then the total charge of the doublets would be zero.

1.1.1 The Expectation of a Fourth Quark

A fourth quark to just fill the last doublet and balance the total fundamental charge was not in itself satisfying. However, arguments arising from the observed weak interactions and experimental results compared to first order QCD calculations suggested a fourth quark.

Figure 1.2: The experimental ratio R as a function of E_{cm} (from reference [3]). R is the ratio of electron–positron annihilation into hadrons and $\mu^+\mu^-$ pairs. For three quarks flavors and three quark colors, $R = 2$; the addition of a fourth quark of charge $+\frac{2}{3}$ increases R to $\frac{10}{3}$ for $E_{cm} > 3$ GeV.

A new quantum number for the quarks, color, was needed to understand the ground states of baryons consisting of three identically flavored quarks without abandoning Fermi-Dirac statistics [2]. One of the early indications that quarks have three colors, came from the experimental ratio of electron–positron annihilation into hadrons and $\mu^+\mu^-$ pairs:

$$R = \frac{\sigma(e^+e^- \to hadrons)}{\sigma(e^+e^- \to \mu^+\mu^-)}. \tag{1.7}$$

To lowest order, $R = N\sum q_i^2$ where q_i is the electric charge of the quark flavor, the sum is over quark flavors which satisfy $2m_i \leq E_{cm}$, and N is the number of quark colors. For the three known quarks, the ratio R was expected to be $\frac{2}{3}$ or 2 depending upon whether there are 1 or 3 quark colors. The experiments [4] found R to be closer to 2 for $E_{cm} \leq 3$ GeV/c^2 and therefore the number of quark colors is 3. This ratio

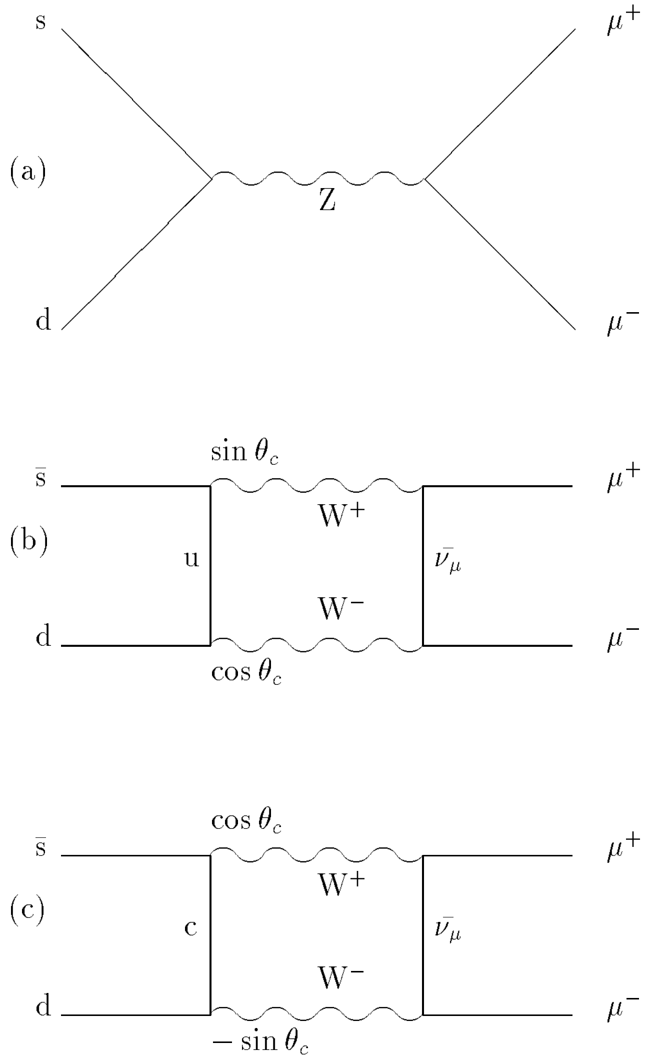

Figure 1.3: Feynman diagrams for $K_L^o \rightarrow \mu^+\mu^-$: (a) unacceptable strangeness changing neutral current, and second order contributions without (b) and with (c) the existence of the charm quark (θ_c is the Cabbibo angle).

can also be used as an indication of the number of quark flavors. Experiments also showed an increase in R above E_{cm} of 3-4 GeV. A fourth quark of $+\frac{2}{3}$ charge increases the expected R to $\frac{10}{3}$. Figure 1.2[1] shows the ratio R as a function of E_{cm}.

The existence of a fourth quark was proposed in 1970 by Glashow, Iliopoulos and Maiani in the "GIM mechanism" [5] to explain the absence of strangeness changing weak neutral currents. The strangeness changing neutral current Feynman diagram shown in figure 1.3a is not acceptable for describing $K_L^o \rightarrow \mu^+\mu^-$. The rate from second order Feynman diagrams, one is shown in figure 1.3b, is too large for the very suppressed $K_L^o \rightarrow \mu^+\mu^-$ branching ratio $\approx 10^{-8}$; the d and s quarks have been Cabbibo mixed [6] $(d\cos\theta_c + s\sin\theta_c)$ and along with the u quark form a doublet. A new quark, in a doublet with $(s\cos\theta_c - d\sin\theta_c)$, introduces second order strangeness changing charged currents, one such Feynman diagram is shown in figure 1.3c. Pairs of second order diagrams, one such pair is the diagrams shown in figure 1.3, do not entirely cancel due to the difference of masses of the up and charm quarks, resulting in the small $B(K_L^o \rightarrow \mu^+\mu^-)$.

1.1.2 Discovery of the J/ψ

The first charmonium state was seen in November 1974 by two experiments. At Brookhaven National Laboratory, the e^+e^-invariant mass in $p + \mathrm{Be} \rightarrow e^+e^- + X$ showed a peak about 3.1 GeV/c^2 [7], figure 1.4; the experimenters named the

[1] A further increase in R as E_{cm} increases comes from $e^+e^- \rightarrow \tau^+\tau^- \rightarrow hadrons$.

Figure 1.4: The e^+e^- invariant mass that constitutes the Brookhaven experiment's J signal (from reference [7]).

new resonance J. Meanwhile researchers at SPEAR (SLAC) [8], saw an energy dependence of the cross section for $e^+e^- \rightarrow hadrons$; a resonance was also identifiable in $e^+e^-$and $\mu^+\mu^-$ final states, figure 1.5, and was named ψ by the experimenters. A third experiment at Frascati [9], was able to immediately reproduce the signal for the particle, which now has the combined name J/ψ.

Immediately it was noticed that the resonance is exceedingly narrow $\ll 1$ MeV, which was much less than the experimental resolutions. Resonances of mass greater than 1 GeV/c^2 have widths between a few MeV and a few hundreds MeV. The J/ψ

Figure 1.5: The energy dependence of the cross section that shows the SPEAR experiment's ψ signal (from reference [8]): a) multi-hadron, b) e^+e^-, and c) $\mu^+\mu^-$ final states.

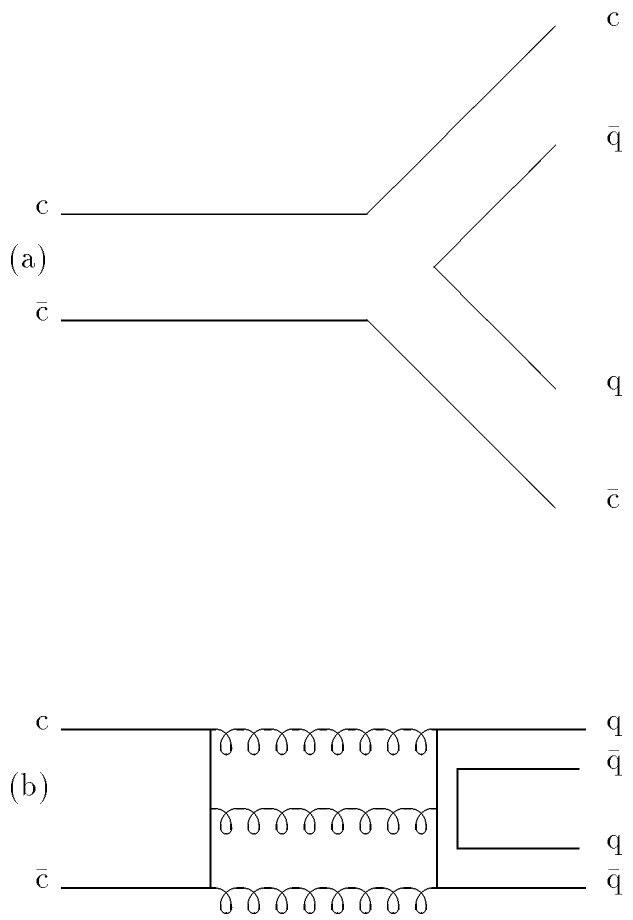

Figure 1.6: Feynman diagrams of strong decays to (a) open charm mesons and (b) light quark mesons. Diagram (a) is OZI-allowed while (b) is OZI-suppressed.

width is 50-1000 times narrower than the other heavy resonances. The best explanation was a new heavy quark forming a new meson, $\bar{c}c$. The narrowness of the J/ψ is attributed to the OZI-rule (Okubo, Zweig and Iizuka) [10, 11, 12]. Strong decays are suppressed since there are no charmed mesons in the final state. To decay into the (eventually identified) lowest mass open charm mesons D^o and $\bar{D}^o$, the charmonium mass must be greater than 3.7 GeV/c^2 ($2M_{D^o}$). A Feynman diagram of a charmonium decay into open charmed mesons is shown in figure 1.6a. In contrast, figure 1.6b shows the OZI-suppressed charmonium decay to light quark mesons. Essentially, disconnected quark-line diagrams are highly suppressed causing any charmonium resonance below the open charm threshold of 3.7 GeV/c^2 to be narrow. Since a meson is a color singlet, at least two gluons are needed; the charge conjugation quantum number for the J/ψ is -1 which requires an odd number of gluons, i.e. a minimum of three gluons is needed for the J/ψ strong decays. Each gluon exchanged between the disconnected quark lines adds to the suppression of the decay.

1.1.3 The Charmonium Spectrum

The radial excitation of the J/ψ, the ψ', was discovered soon afterward below the open charm threshold. Other narrow resonances of charmonium bound states were expected with different spin and angular momentum quantum numbers below the open charm threshold[2]. Each charmonium state constituent has an intrinsic spin quantum number of $\frac{1}{2}$. The two fermions combine for a total spin quantum number $S = 0, 1$. Each bound state can be labelled by conventional spectroscopic notation $^{2S+1}\mathrm{L}_J$ where L is the orbital angular momentum denoted by S, P, D, F... for $L = 0$, 1, 2, 3... and J is the total spin. The charmonium states can also be characterized by the quantum numbers for total spin J, parity P, and charge conjugation C, and denoted by J^{PC}. For fermion-antifermion systems, the parity and charge conjugation

[2]The $J = 2$ D states are expected to be narrow even though their masses are expected to be above the open charmed threshold. Parity forbids either state to decay into $\bar{D}D$; both states could decay to DD^* if the mass is greater than 3875 MeV/c^2.

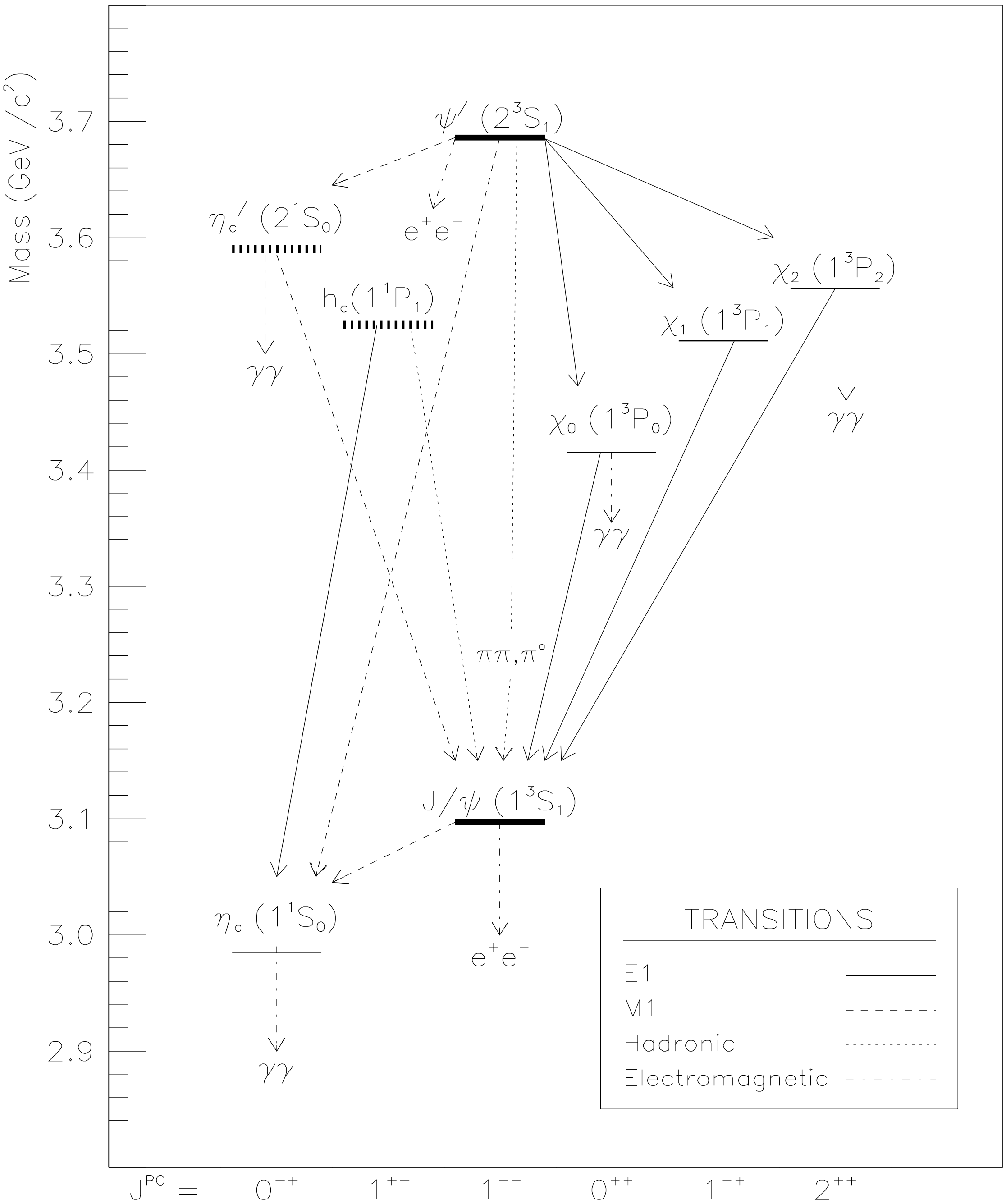

Figure 1.7: The charmonium spectrum below the open charm threshold with the $^1P_1$ located at the spin weighted average of the triplet P wave states. Thick solid lines denote the states which are directly produced by e^+e^- annihilation; states which were unseen or needed to be verified before this experiment are represented by thick broken lines. The known and expected hadronic and electromagnetic transitions and decays that E760 can detect are shown.

are

$$P = (-1)^{L+1} \tag{1.8}$$

$$C = (-1)^{L+S}. \tag{1.9}$$

The J/ψ and ψ' were first formed in e^+e^-annihilation; the intermediate virtual photon of the process dictates that the quantum numbers of the J/ψ and ψ' are $J^{PC} = 1^{--}$. Other charmonium states have been observed through decays of the J/ψ and ψ' (section 1.4) and by direct formation in $\bar{p}p$ collisions (section 1.5). All expected charmonium states below the open charm threshold have been seen through the e^+e^- collisions[3] except the $^1\mathrm{P}_1$. The charmonium spectrum is shown in figure 1.7 with the $^1\mathrm{P}_1$ located at the spin weighted center of gravity of the triplet P states (χ_0, χ_1, and χ_2), see section 1.2.2.

1.2 Theory

QCD is analogous to QED (quantum electrodynamics). In QED, charged particles exchange massless photons; color charged particles exchange massless gluons in QCD. Whereas the photon of QED does not have electrical charge, there are eight different colored gluons in QCD. QCD allows gluons to self-couple and results in confinement (i.e., no unbound quarks or gluons).

[3]The η_c' needs to be verified. See section 1.4, figure 1.10.

The hydrogen atom and positronium have been the testing grounds for QED and for relativistic corrections. QED has been very successful in describing the hydrogen atom. The e^+e^- bound states of positronium are analogous to $\bar{c}c$ bound states of charmonium. Both charmonium and bottomonium, $\bar{b}b$ provide testing grounds for QCD.

Proposed potentials and methods for calculating quantities of the charmonium system vary. Below are descriptions of the general characteristics of potentials and calculational methods. In general, non-relativistic potentials are used with relativistic corrections leading to spin dependent contributions.

1.2.1 Potentials

At short distances, single gluon exchange is approximated by a Coulomb-like interaction

$$V_{short}(r) = -\frac{4}{3}\frac{\alpha_s(r)}{r}; \tag{1.10}$$

this is similar to QED with the exception of a separation distance dependent fine structure constant $\alpha_s(r)$, as compared to $\alpha = \frac{1}{137}$, and a factor of $\frac{4}{3}$ which arises from requiring the quark-antiquark to be in a singlet color state. The strong fine structure constant can be stated in momentum-space as

$$\alpha_s(Q^2) = \frac{12\pi}{(33 - 2n_f)\ln(Q^2/\Lambda^2)}, \tag{1.11}$$

where n_f is the number of fermion flavors with mass below Q and Λ is a characteristic scale (generally taken to be of the order of 200 MeV). The logarithmic dependence of

α_s causes the gluon exchange to be weaker at short distances. The quasi-free behavior of quarks at short distances (large momentum transfer) is called *asymptotic freedom*.

Since there have been no free quarks or gluons observed, it is believed that quarks and gluons are confined. As the distance between quarks increases, the potential increases; an arbitrary form is linear,

$$V_{long}(r) = kr \tag{1.12}$$

where k is a force constant about 1 GeV/fm.

The two extreme distance potentials can be combined simply into

$$V(r) = -\frac{4}{3}\frac{\alpha_s(r)}{r} + kr \tag{1.13}$$

which is called the "Cornell potential" [13]. In momentum space, Richardson [14] proposed the potential

$$V(Q^2) = -\frac{4}{3}\frac{12\pi}{(33-2n_f)}\frac{4\pi}{Q^2}\frac{1}{\ln(1+Q^2/\Lambda^2)}; \tag{1.14}$$

for large Q^2 (small r) the potential behaves as $[\ln(Q^2/\Lambda^2)]^{-1}$ and for small Q^2 (large r) the behavior is Q^{-4}, corresponding to a linear potential. There are other forms of potentials, e.g. purely logarithmic $V(r) = a\ln(r/r_\circ)$, power laws $V(r) = b + cr^\nu$ and combinations of any of the above. For the most part, calculations are done with modified Cornell and Richardson potentials and reproduce the gross $\bar{c}c$ spectra fairly well. As shown in figure 1.8, the potentials behave similarly for distances between 0.1 and 1 fm, the range of $\bar{c}c$ distances for charmonium.

Figure 1.8: The comparison of several potentials shows the same behavior for the relevant separation distance for the charmonium system (from reference [15]).

The modified potentials add parameters to the potential which are usually motivated by QCD concerns. Generally, the Hamiltonian is expanded in $(\frac{v}{c})^2$ as

$$H = H_0 + H_1 + \cdots . \tag{1.15}$$

The nonrelativistic Hamiltonian is

$$H_0 = \frac{p^2}{m} + V_s(r) + V_v(r), \tag{1.16}$$

where p and m are respectively the quark momentum and mass, $V_v(r)$ is a vector-like potential, and $V_s(r)$ is a scalar-like potential. The short range one gluon exchange is in V_v. The long range confining potential cannot be entirely vector-like [16, 17]. The confinement potential is usually taken to be V_s; there can be a vector-like contribution to the confinement potential which would be included in V_v.

The first order term in $(\frac{v}{c})^2$ of the Hamiltonian can be split into a spin independent term H_{SI} and a spin dependent term H_{SD}:

$$H_1 = H_{SI} + H_{SD}. \tag{1.17}$$

The spin independent Hamiltonian is

$$\begin{aligned} H_{SI} = \quad & -\tfrac{p^4}{4m^3} + \tfrac{1}{4m^2}\{\tfrac{2L(L+1)}{r}V_v' + [p^2, V_v - rV_v'] \\ & +2(V_v - rV_v')p^2 + \tfrac{1}{2}(\tfrac{8}{r}V_v' + V_v'' - rV_v''')\}, \end{aligned} \tag{1.18}$$

where the prime ($'$) indicates a derivative with respect to the separation distance r. The spin dependent Hamiltonian is discussed in the next section.

1.2.2 Spin Dependence

The spin dependent Hamiltonian can be split into three terms,

$$H_{SD} = H_{SO} + H_T + H_{SS} \tag{1.19}$$

where the indices SO, T and SS refer to spin-orbit, tensor and spin-spin terms, respectively. These terms were first considered by Pumplin et al. [18] and Schnitzer [19] and are

$$H_{SO} = \quad \tfrac{1}{2m^2 r}(3V_v' - V_s')\langle \vec{L} \cdot \vec{S} \rangle \quad = V_{SO}\langle \vec{L} \cdot \vec{S} \rangle, \tag{1.20}$$

$$H_T = \quad -\tfrac{1}{m^2}(V_v'' - \tfrac{V_v'}{r})\langle T_{12} \rangle \quad = V_T \langle T_{12} \rangle, \tag{1.21}$$

$$H_{SS} = \quad \tfrac{2}{3m^2}(\nabla^2 V_v)\langle \vec{S_1} \cdot \vec{S_2} \rangle \quad = V_{SS}\langle \vec{S_1} \cdot \vec{S_2} \rangle, \tag{1.22}$$

where

$$T_{12} = \frac{1}{3}[3(\vec{S_1} \cdot \hat{r})(\vec{S_2} \cdot \hat{r}) - \vec{S_1} \cdot \vec{S_2}]. \tag{1.23}$$

The expectation values are

$$\langle \vec{L} \cdot \vec{S} \rangle = \tfrac{1}{2}[J(J+1) - L(L+1) - S(S+1)], \tag{1.24}$$

$$\langle T_{12} \rangle = \frac{-\langle \vec{L}\cdot\vec{S}\rangle^2 - \frac{1}{2}\langle \vec{L}\cdot\vec{S}\rangle + \frac{1}{3}\langle \vec{L}^2\rangle\langle \vec{S}^2\rangle}{(2L+3)(2L-1)}, \tag{1.25}$$

$$\langle \vec{S}_1 \cdot \vec{S}_2 \rangle = \tfrac{1}{2}[S(S+1) - \tfrac{3}{2}]. \tag{1.26}$$

The P wave states are $L = 1$ and the triplet P wave masses are

$$M_{\chi_0} = M_{SI} - 2V_{SO} - \tfrac{1}{3}V_T + \tfrac{1}{4}V_{SS}, \tag{1.27}$$

$$M_{\chi_1} = M_{SI} - V_{SO} + \tfrac{1}{6}V_T + \tfrac{1}{4}V_{SS}, \tag{1.28}$$

$$M_{\chi_2} = M_{SI} + V_{SO} - \tfrac{1}{30}V_T + \tfrac{1}{4}V_{SS} \tag{1.29}$$

where M_{SI} is from equation 1.18, the spin independent Hamiltonian. The singlet P wave mass is

$$M_{h_c} = M_{SI} - \frac{3}{4}V_{SS}. \tag{1.30}$$

The last four equations can be inverted to find the spin-orbit, tensor, spin-spin and spin independent contributions to the P wave masses:

$$V_T = -\tfrac{5}{3}M_{\chi_0} + \tfrac{5}{2}M_{\chi_1} - \tfrac{5}{6}M_{\chi_2}, \tag{1.31}$$

$$V_{SO} = -\tfrac{1}{6}M_{\chi_0} - \tfrac{1}{4}M_{\chi_1} + \tfrac{5}{12}M_{\chi_2}, \tag{1.32}$$

$$V_{SS} = M_{\chi_{cog}} - M_{h_c}, \tag{1.33}$$

$$M_{SI} = \tfrac{3}{4}M_{\chi_{cog}} + \tfrac{1}{4}M_{h_c}, \tag{1.34}$$

where $M_{\chi_{cog}}$ is the spin weighted average of the triplet P wave states:

$$M_{\chi_{cog}} = \frac{\sum(2J+1)M_{\chi_J}}{\sum(2J+1)} = \frac{1M_{\chi_0} + 3M_{\chi_1} + 5M_{\chi_2}}{9}. \tag{1.35}$$

The triplet P wave mass differences are caused by spin-orbit and tensor contributions. Only the spin-spin, or hyperfine, contribution causes the M_{h_c} to be non-degenerate with $M_{\chi_{cog}}$.

The Hamiltonian described above is an expansion to first order in $(\frac{v}{c})^2$; higher order terms may have non-negligible contributions. The virial theorem is used to show the importance of the higher order terms. The expectation value for the kinetic energy $\langle T\rangle$ is

$$\langle T\rangle = \frac{1}{2}\langle\vec{r}\cdot\vec{\nabla}V(\vec{r})\rangle. \tag{1.36}$$

Assuming a linear distance term dominates at the mean radius of the charmonium system, then $2\langle T\rangle = \langle V\rangle$ or $E_b = 3\langle T\rangle$ (where E_b is the binding energy of the system, $\langle T\rangle + \langle V\rangle$). Using the non-relativistic expression

$$\langle T\rangle = 2\left(\frac{m_c\langle v^2\rangle}{2}\right), \tag{1.37}$$

the expectation for the square of the velocity is

$$\langle v^2\rangle = \frac{E_b}{3m_c}, \tag{1.38}$$

where m_c is the mass of the charm quark. A binding energy of 675 MeV ($= M_{\psi'} - M_{J/\psi}$) and $m_c = 1.5$ GeV/c^2 leads to the estimation that

$$\langle v^2\rangle \approx 0.15c^2. \tag{1.39}$$

This rough estimate shows that the charmonium system is not completely non-relativistic and that relativistic effects (for example spin dependence) can be important.

1.3 Expectations of the $^1P_1$

Below are summaries of the theoretical expectations for the $^1P_1$ mass, different decay rates and total width. In general, the predictions are based on a potential and calculational method which depend upon a set of parameters. The parameters are determined by fits to existing charmonium (and in some cases bottomonium) experimental data. The summaries are not complete but are presented to give an idea of the many calculations that have been done.

1.3.1 Mass

Using E760's measurement of the χ_1 and χ_2 masses [20] (3510.53 ± 0.13 MeV/c^2 and 3556.15 ± 0.14 MeV/c^2, respectively) and the previously measured average χ_0 mass [21] (3415.1 ± 1.0 Mev/c^2), the spin weighted average mass is

$$M_{\chi_{cog}} = 3525.27 \pm 0.23 \text{ MeV/c}^2. \tag{1.40}$$

The mass difference between the $^1P_1$ and χ_{cog} arises entirely from the hyperfine splitting as shown above. The hyperfine mass splitting is defined here as

$$\Delta_{HF} = -V_{SS} = M_{h_c} - M_{\chi_{cog}}. \tag{1.41}$$

There are a few theoretical papers (for example, references [22, 23, 24]) which predict the singlet state to be degenerate with χ_{cog}, $\Delta_{HF} = 0$.

Early predictions of the $^1P_1$ mass tended to have Δ_{HF} negative. One of the first simple potential model calculations [25] resulted in $\Delta_{HF} = -9$ MeV/c^2; another

Authors	Δ_{HF} (MeV/c^2)	Comment
Gupta et al. [28]	1.4	
Gupta et al. [29]	2.0	Semi-relativistic potential
Gupta et al. [30]	-4.5	
McClary & Byers [31]	5	
Ono & Schöberl [32]	-10	Fit includes light quark mesons
Pantaleone & Tye [33]	1.4	
Badalyan & Yurov [34]	8.0	VCM with $\sigma_1 < 0$
Badalyan & Yurov [34]	1.13	VCM with $\sigma_1 \approx 0$
Badalyan & Yurov [34]	-1.8	VCM with $\sigma_1 > 0$
Halzen et al. [35]	0.7 ± 0.2	
Dixit et al. [36]	-7.3 to 0	Power law
Galkin et al. [37]	-1	
Fulcher [38]	3	
Lichtenberg et al. [39]	-4.1	
Lichtenberg & Potting [40]	-2.9 to 5.4	
Olsson & Suchyta [41]	-4.6	2 spin independent terms
Igi & Ono [42, 43]	1.91 to 3.49	2 loop correction
Chen & Kuang [44]	0.89 to 1.80	2 loop correction

Table 1.1: Theoretical predictions for the hyperfine mass splitting, Δ_{HF}. See the references for more information about the potentials and methods.

calculation [26] resulted in a splitting of -22 MeV/c^2. A modified Coulomb potential [27], which does not satisfy confinement for large r, predicted $\Delta_{HF} = 58$ MeV/c^2.

From the early 1980's until the present, there have been many potentials tried. In table 1.1 is a list of predictions made by theorists; included are comments about the specific potentials used or methods employed, see the individual references for details. As can be seen in table 1.1, Δ_{HF} is predicted to be a few MeV/c^2 and most predictions have Δ_{HF} positive, i.e. mass of the $^1P_1$ is greater than $M_{\chi_{cog}}$.

Author	$\Gamma_{h_c \to \gamma \eta_c}$ (keV)	Comments
Renard [45]	240	
Galkin [37]	559	
Novikov et al. [46]	975	
McClary & Byers [31]	483	Nonrelativistic 660 keV
Chao et al. [47]	385	Nonrelativistic 650 keV
Bodwin et al. [48]	450	Scaling to $\Gamma_{\chi \to \gamma J/\psi}$
Casalbuoni et al. [49]	450	

Table 1.2: Theoretical predictions for the $^1\mathrm{P}_1$ (h_c) radiative transition to η_c.

1.3.2 Decay Rates

The expected total width of the $^1\mathrm{P}_1$ is expected to be narrow, $\leq 1\ MeV$. The contributions from radiative and hadronic decays are expected to be nearly the same, with the dominant decay expected to be $\eta_c\gamma$. Most calculations relate the partial widths of the $^1\mathrm{P}_1$ to the already measured partial widths of other charmonium states.

The radiative transition to the η_c has been calculated several times. In the non-relativistic limit, the transition rate is

$$\Gamma(^1\mathrm{P}_1 \to \eta_c\gamma) = \frac{4\alpha e_c^2 E_\gamma^3}{9} \mid \langle f|r|i\rangle \mid^2, \tag{1.42}$$

where e_c is the electric charge of the charm quark, E_γ is the energy of the radiative gamma ray, and the matrix element involves the normalized initial and final state wave functions. The wave functions are model dependent and vary slightly. Table 1.2 shows a few of the theoretical predictions. Bodwin, Braaten and Lepage [48] predict the radiative transition by scaling (using the photon energies) to the $\chi_{0,1,2}$ radiative decays to J/ψ. Coupled channel effects (influence from the open charm threshold) may decrease the radiative width; a 10% decrease has been predicted of the radiative

Authors	$\Gamma_{h_c \to J/\psi\pi\pi}$ (keV)	Comments
Kuang et al. [50]	4.12 (8.24)	Multipole expansion
Chemtob & Navelet [51]	52.6	Semi-perturbative
Chen & Yi [52]	7.1 (14.2)	Multipole, 2 loop
Chen & Yi [52]	4.1 (9.3)	Use Kuang's potential [50]

Table 1.3: Theoretical predictions for the $^1P_1$ (h_c) hadronic transition to $J/\psi\pi\pi$. The multipole expansion widths are for $\alpha_E = \alpha_M$ ($\alpha_E = 2\alpha_M$), see references for details.

widths of the triplet P wave states [13]. Renard also predicts that the M1 transition to the triplet P states is a few keV [45], a small contribution to the total width.

The hadronic transitions from the $^1P_1$ to $J/\psi + X$ are only allowed energetically for X being π^o, $\pi^o\pi^o$, or $\pi^+\pi^-$. A hadronic transition via η is not allowed since $M\eta > M_{\chi_{cog}} - M_{J/\psi}$. Tables 1.3 and 1.4 show predictions for the $\pi\pi$ and π^o transitions, respectively. All of the authors predict the $J/\psi\pi\pi$ width to be greater than the $J/\psi\pi^o$ width.

The $^1P_1$ inclusive partial widths to hadrons (radiative decay to hadrons) is really the partial width to three gluons (gamma ray and two gluons) where the gluons automatically hadronize. A simple scaling to a known partial width was first done

Authors	$\Gamma_{h_c \to J/\psi\pi^o}$ (keV)	Comments
Kuang et al. [50]	2	Multipole expansion
Chemtob & Navelet [51]	0.0061	Semi-perturbative
Chen & Yi [52]	0.58 (1.16)	Multipole, 2 loop
Chen & Yi [52]	0.29 (0.57)	Use Kuang's potential [50]

Table 1.4: Theoretical predictions for the $^1P_1$ (h_c) isospin violating hadronic transition to $J/\psi\pi^o$. The multipole expansion widths are for $\alpha_E = \alpha_M$ ($\alpha_E = 2\alpha_M$), see references for details.

Authors	$\Gamma_{h_c \to hadrons}$ (keV)	Comments
Renard [45]	120	
Novikov [46]	60 to 350	
Kuang et al. [50]	53.7	Multipole expansion
Chen & Yi [52]	19.3 (35)	Multipole, 2 loop
Chen & Yi [52]	51 (51)	Use Kuang's potential [50]
Bodwin et al. [48]	530	Factorization theorm

Table 1.5: Theoretical predictions for the $^1\mathrm{P}_1$ (h_c) hadron decays. The multipole expansion widths are for $\alpha_E = \alpha_M$ ($\alpha_E = 2\alpha_M$), see references for details.

by Barbieri, Gatto and Remiddi [53]:

$$\frac{\Gamma(^1\mathrm{P}_1 \to \mathrm{hadrons})}{\Gamma(\chi_1 \to \mathrm{hadrons})} \simeq \frac{5}{2n_f}, \tag{1.43}$$

where $n_f = 3$ is the number of quark flavors in the final state hadrons. The theoretical predictions of the partial width to hadrons is given in table 1.5. Bodwin, Braaten and Lepage [48] also uses the known χ_1 partial width to hadrons to predict the $^1\mathrm{P}_1$ radiative partial width to hadrons:

$$\frac{\Gamma(^1\mathrm{P}_1 \to \gamma + \mathrm{hadrons})}{\Gamma(\chi_1 \to \mathrm{hadrons})} \simeq \frac{6e_c^2\alpha}{n_f\alpha_s(M_c)}. \tag{1.44}$$

Table 1.6 shows the predicted $^1\mathrm{P}_1$ radiative transitions to hadrons. Both the hadronic and radiative transition to hadrons decays are OZI suppressed.

Authors	$\Gamma_{h_c \to \gamma + hadrons}$ (keV)	Comments
Renard [45]	210	
Novikov [46]	7 to 40	
Kuang et al. [50]	5.91	Multipole expansion
Chen & Yi [52]	2.1 (3.7)	Multipole, 2 loop
Chen & Yi [52]	5.7 (5.5)	Use Kuang's potential [50]
Bodwin et al. [48]	15	Factorization theorm

Table 1.6: Theoretical predictions for the $^1\mathrm{P}_1$ (h_c) radiative decays to hadrons. The multipole expansion widths are for $\alpha_E = \alpha_M$ ($\alpha_E = 2\alpha_M$), see references for details.

Author	Γ_{h_c} (keV)
Renard [45]	500 to 1000
Kuang et al. [50]	394
Chen & Yi [52]	360
Bodwin et al. [48]	980

Table 1.7: Theoretical predictions for the ${}^1\mathrm{P}_1$ (h_c) total width.

To find the ${}^1\mathrm{P}_1$ partial width to $\bar{p}p$, Kuang et al. uses the η_c partial width:

$$\frac{\Gamma({}^1\mathrm{P}_1 \to \bar{p}p)}{\Gamma(\eta_c \to \bar{p}p)} \simeq \frac{\Gamma({}^1\mathrm{P}_1 \to \text{hadrons})}{\Gamma(\eta_c \to \text{hadrons})}; \tag{1.45}$$

they predict a partial width of 0.186 keV. Chen & Yi predict 0.044 keV. If equation 1.43 is used, then the $\bar{p}p$ partial width of the ${}^1\mathrm{P}_1$ is 0.64 keV.

Authors give total widths which are the sum of the partial widths. Some authors add other author's partial widths to their own widths to arrive at a prediction for the ${}^1\mathrm{P}_1$ total width. Table 1.7 shows the theoretical ${}^1\mathrm{P}_1$ total width predictions.

1.4 Spectroscopy by e^+e^- Annihilations

The majority of charmonium spectroscopy has been done using e^+e^- colliders, from the discovery of the charm quark until the middle of the 1980's. Only $\bar{c}c$ states with the same quantum number as the intermediate virtual photon, $J^{PC} = 1^{--}$, can be made directly from e^+e^- annihilations, figure 1.9a. Interactions involving e^+e^- can produce even J $\bar{c}c$ states through two intermediate photons (figure 1.9b), which introduces an additional factor of α^2 in the rate causing the production rate to be 10^{-4} smaller than any one intermediate photon rate. Since $C = -1$ for the ${}^1\mathrm{P}_1$, three

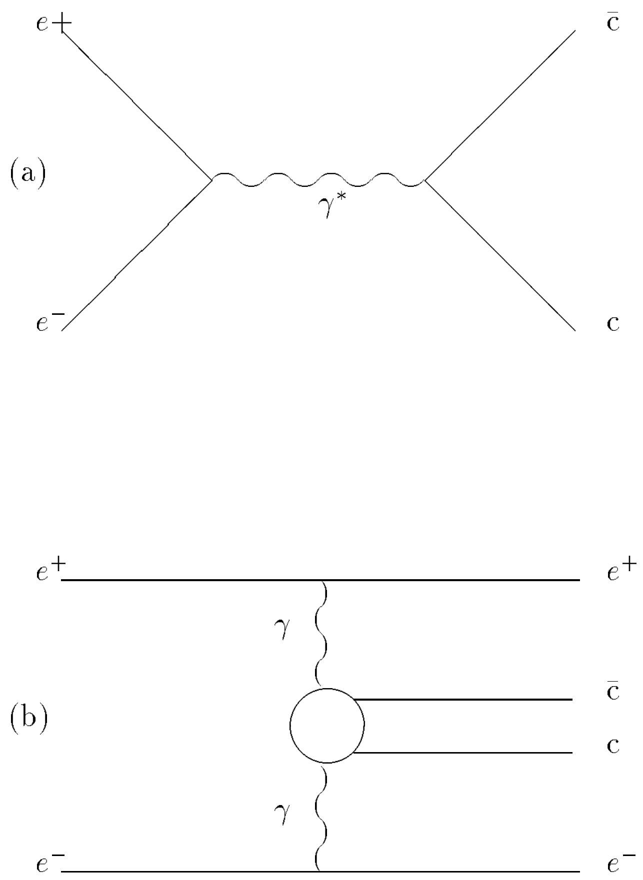

Figure 1.9: Feynman diagrams of direct production of charmonium in e^+e^- annihilation: (a) 1^{--} $\bar{c}c$ states by one virtual photon and (b) even J $\bar{c}c$ states by two intermediate photons.

intermediate photons are needed, which thereby decreases the production rate even more.

Spectroscopy of the $\bar{c}c$ states with quantum numbers other than the photon has been done through the decays of the 1^{--} $\bar{c}c$ states produced by e^+e^- interactions, in particular radiative transitions. The determination of the characteristics of the non-1^{--} $\bar{c}c$ states depends upon an experiment's ability to measure the energy of the decay particle(s). An e^+e^- experiment, Crystal Ball [54], has been able to measure the radiative photons from $\psi' \rightarrow {}^3\mathrm{P}_{0,1,2}$ (${}^3\mathrm{P}_{0,1,2}$ are known as $\chi_{0,1,2}$) and the subsequent

Figure 1.10: The inclusive photon spectrum from the ψ' seen by Crystal Ball (from reference [54]).

radiative transition $^3\mathrm{P}_{0,1,2} \to J/\psi$ which are all E1 transitions. Crystal Ball has also seen evidence of M1 transitions $J/\psi \to \gamma\eta_c$ (the radiative transition from the triplet S state to the singlet S state) and $\psi' \to \gamma\eta_c'$[4] as well as the hindered M1 transition[5] $\psi' \to \gamma\eta_c$. The inclusive photon spectrum from the ψ' is shown in figure 1.10, as obtained by the Crystal Ball Experiment. Charge conjugation invariance prohibits the ψ' to radiatively decay to the $^1\mathrm{P}_1$.

[4]The η_c' signal is not very strong since the measured energy of the photon is near the threshold of Crystal Ball's detector. The η_c' needs to be verified.

[5]The transition changes principal quantum number; a radially excited state decays into a non-excited state of charmonium.

The $^1P_1$ can only be a decay product of radiative decays of η_c' (E1) and ^3P (M1), depending upon the $^1P_1$ mass. The expected radiative decays of the $^1P_1$ are to η_c (E1) and ^3P (M1), again depending upon the $^1P_1$ mass. Note that the expected small difference of masses between the singlet and triplet P wave states should result in very small radiative rates for such M1 transitions. Crystal Ball searched for the $^1P_1$ through the isospin violating transition $\psi' \to {}^1P_1\pi^o$ [55]; the π^o energy spectrum was studied and no signal was found corresponding to a mass between the J/ψ mass and 3.55 GeV/c^2 ($= M_{\psi'} - M_{\pi^o}$).

1.5 Spectroscopy by $\bar{p}p$ Annihilations

The CERN ISR (Intersecting Storage Ring) R704 experiment was able to directly form and study some of the $J^{PC} \neq 1^{--}$ $\bar{c}c$ states in $\bar{p}p$ collisions before the ISR was shut down in 1984. R704 pioneered $\bar{p}p$ spectroscopy using a cooled $\bar{p}$ beam and a hydrogen gas jet [56]. The two-armed, nonmagnetic detector (geometrical acceptance $\approx$ 12%) used by R704 investigated the electromagnetic decay products of several charmonium states. In particular,

$$\bar{p}p \to \bar{c}c \to \quad e^+e^- + X \tag{1.46}$$

$$\bar{p}p \to \bar{c}c \to \quad \gamma\gamma \tag{1.47}$$

where the $e^+e^-(\gamma\gamma)$ invariant mass reconstructs to a $\bar{c}c$ state J/ψ or ψ' (η_c or χ_2). For the first time, the 0^{-+}, 1^{++} and 2^{++} charmonium states (η_c, χ_1 and χ_2, respectively) were formed directly. Figure 1.11 show the diagrams for two and three intermediate

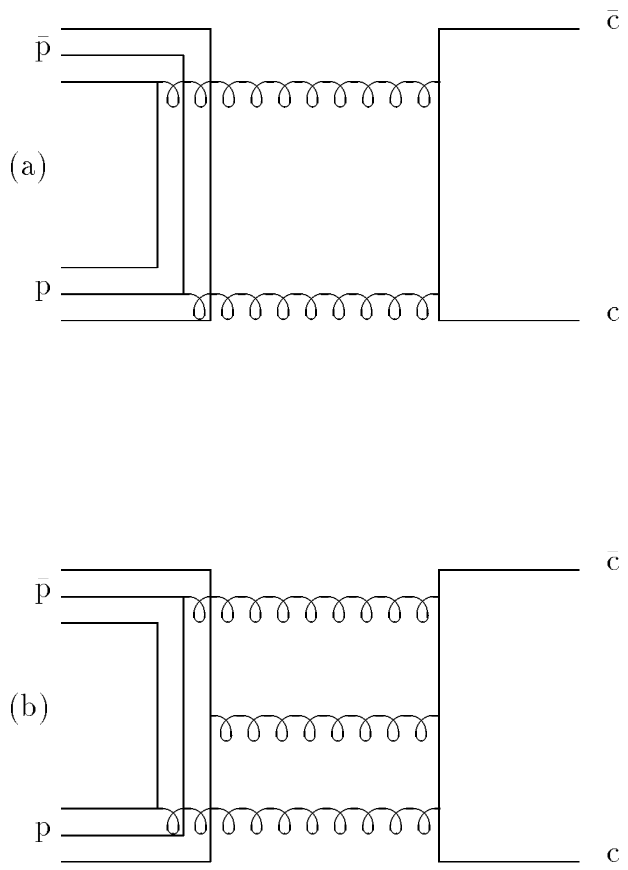

Figure 1.11: The Feynman diagrams of $\bar{c}c$ states produced in $\bar{p}p$ annihilation: (a) two intermediate gluons to form even J $\bar{c}c$ states and (b) three intermediate gluons to form odd J $\bar{c}c$ states.

gluons for forming $\bar{c}c$ states in $\bar{p}p$ annihilations. Near the spin weighted center of gravity of the ^{3}P states, five $J/\psi + X$ candidates were seen [57]. These events can be interpreted as possible evidence for a resonance; a discussion of the five events is presented in section 8.5.

The hard part of doing charmonium spectroscopy with $\bar{p}p$ annihilations is extracting the charmonium signal. Figure 1.12 shows the total $\bar{p}p$ cross section in the charmonium energy range is near 60 mb. The largest expected peak cross section for a charmonium state with an electromagnetic final state ($\bar{p}p \rightarrow J/\psi \rightarrow e^+e^-$) is 360 nb.

Figure 1.12: The total cross section for $\bar{p}p$ interactions (from reference [58]).

The electromagnetic decay signatures of bound charmonium result in rates that are at least 10^5 smaller than the total $\bar{p}p$ interaction rate. The advantage is that the determination of resonance characteristics, mass and width, are not dependent upon detector resolution but upon knowledge of the $\bar{p}$ momentum and spread of momentum. R704 proved that $\bar{c}c$ states can be separated from the large background and improved the knowledge of the non 1^{--} states.

E760 is modelled after R704. The Fermilab Antiproton Accumulator allows for a factor of 10 increase in the luminosity. Whereas the R704 detector was a two-armed spectrometer, the E760 detector covers the full azimuth and has a larger polar angular acceptance. The overall detector acceptance is 4 to 5 times larger than the

R704 detector. E760's proposed purpose has been to further study the η_c, χ_1 and χ_2 as well as search for the $^1\mathrm{P}_1$ and η_c'. E760 uses the electromagnetic decay signatures, equations 1.3 and 1.4, as the main approach to search for $\bar{c}c$ states.